Biosensors and Bioelectronics 132 (2019) 217–223

Contents lists available at ScienceDirect

Biosensors and Bioelectronics

journal homepage: www.elsevier.com/locate/bios

Highly electrocatalytic biosensor based on Hemin@AuNPs/reduced graphene oxide/chitosan nanohybrids for non-enzymatic ultrasensitive detection of hydrogen peroxide in living cells

Wenjing Wang[a], Huabiao Tang[b], Yuan Wu[a], Yinli Zhang[b], Zhaohui Li[b,*]

[a] Institute of Chemical Biology and Nanomedicine, College of Chemistry and Chemical Engineering, Hunan University, Changsha 410082, China
[b] College of Chemistry and Molecular Engineering, Zhengzhou University, Zhengzhou 450001, China

ARTICLE INFO

Keywords:
Hemin
Biomineralization
Gold nanoparticles
Enzymatic-free assay
Hydrogen peroxide
Living cell

ABSTRACT

A non-enzymatic and highly electrocatalytic H_2O_2 biosensor was proposed by using a novel electrode composed of hemin-capped biomineralized gold nanoparticles (Hem@AuNPs), reduced graphene oxide (rGO) and chitosan (CS). Owing to the excellent electrocatalytic activity of Hem@AuNPs and great conductivity of rGO, this developed biosensor is capable of ultrasensitive measuring H_2O_2 in real-time. In addition, the introduction of CS resulted in a film on the electrode, which can enhance the stability by protecting the biosensor from external disturbances. Taking advantages of the peroxidase-like activities of the nanohybrids, the developed electrode exhibited outstanding electrochemical performance toward H_2O_2 with high selectivity, fast response, superior sensitivity and good stability. More importantly, the lower determination limit of 9.3 nM and wider linear ranges of 5 orders of magnitude enable this biosensor to detect H_2O_2 releasing from living Hela cells accurately. This work provides tremendous potential for real-time monitoring the secretion of H_2O_2 in living cells.

1. Introduction

Reactive oxygen species (ROS) in cell play important roles in various physiological and pathological processes. In normal cells, ROS can regulate signal transmission and physiological state (Fleury et al., 2002), and the excessive ROS can be eliminated by the anti-oxidization system. However, if the anti-oxidization system is out of balance with the production of ROS, it will give rise to oxidative stress (Wei, 1998). Oxidative stress can cause chaotic intracellular signaling, cell membrane damage, cell ion communication damage, and cell membrane lipid peroxidation (Halliwell and Chirico, 1993), which might result in organ damage and tumor diseases. H_2O_2 is one of the most important ROS in cell. Previous research has shown that the increase of H_2O_2 in cells can directly or indirectly induce cell malignant transformation, and keep the malignant phenotype of tumor cells (Valko et al., 2004). Compared to normal cells, tumor cells accumulate large amounts of H_2O_2 (Lim et al., 2005). During the carcinogenesis process of normal cells, a large amount of H_2O_2 are produced, which could cause sustained oxygen stress and lead to DNA oxidative damage. If the DNA damage is not repaired in time, some genes related to tumorigenesis will be activated and passaged by cell division, leading to malignant transformation of normal cells and triggering the tumors (Valavanidis et al., 2009). In other words, once normal cells begin to transform into tumor cells, they have the ability to produce larger amounts of H_2O_2. Therefore, the massive production of H_2O_2 is considered as one of the key factors in the process of carcinogenesis (Policastro et al., 2004). Hence, it is in dire need to develop a rapid, stable, and accurate method to detect the H_2O_2 releasing from living cells.

Up to now, many analytical methods have been established to detect H_2O_2, including spectrophotometry (He et al., 2017), chromatography (Song et al., 2017), fluorometry (Hu et al., 2014), chemiluminescence (Lebiga et al., 2015) and electrochemical technologies (Chen et al., 2018). Among them, electrochemical techniques have been widely used in real-time and in situ detection of H_2O_2 due to the advantages of high sensitivity and quick response. Some natural enzymes, for example, horseradish peroxidase (HRP) (Santos and Maia, 2012), have been widely used in electrochemical biosensor because of their high efficiency, good selectivity and excellent catalytic activity towards H_2O_2. However, the enzyme-based H_2O_2 biosensors have some disadvantages, such as expensive, unstable, difficult to immobilization and easy to inactivation, which limit their further application. So it is necessary to develop the peroxidase mimics and non-enzymatic H_2O_2 biosensors.

In recent years, the materials with peroxidase-like activity have attracted great attention of researchers, including transition metal

* Corresponding author.
E-mail address: zhaohui.li@zzu.edu.cn (Z. Li).

https://doi.org/10.1016/j.bios.2019.02.039
Received 12 December 2018; Received in revised form 2 February 2019; Accepted 15 February 2019
Available online 21 February 2019
0956-5663/

sulfides (Wang et al., 2013), carbon material (Bhunia et al., 2018), metallic oxide (Jha et al., 2014), noble metal nanomaterials (Gupta et al., 2018) and so on. Among the noble metal nanoparticles, AuNPs (Berbec et al., 2018) have been witnessed a persistent utilization in electrochemical biosensor because of its good biocompatibility and excellent conductivity. Especially, AuNPs exhibit excellent electrocatalytic activity towards the reduction of H_2O_2. Graphene (GR) (Drmosh et al., 2019) is also one of the most popular candidates to catalyze the electrochemical reduction of H_2O_2 due to its outstanding properties such as high electrical conductivity, large surface area and admirable stability. Hemin (Hem), an iron porphyrin derivative, has also been shown to have electrocatalytic abilities towards H_2O_2 based on the redox reaction of iron in the core (Cao et al., 2018; Ye et al., 2017). However, direct application of Hem is limited by its poor dispersion activity (Zhang et al., 2014) and weak conductivity (Wang et al., 2017).

In order to fasten the materials on electrode more tightly, it is necessary to add an adhesive to the modified materials. Chitosan (CS) is a polycationic polymer. Because of the excellent film-forming ability, good biocompatibility, outstanding permeability and high adhesion, CS has been widely used to immobilize various modified materials on the electrode surface, which can form a stable film to protect the electrode materials (Chang et al., 2017; Li et al., 2017; Rizwan et al., 2018). Given the poor conductivity of CS, combination with high conductive nanomaterials makes it suitable for the fabrication of electrochemical biosensors (Afkhami et al., 2017; Pakchin et al., 2018). For instance, CS was widely used in the H_2O_2 electrochemical sensor together with various conductive nanomaterials such as graphene, carbon nanotubes, and metal nanoparticles (Bai et al., 2016; Luo et al., 2005; Zhai et al., 2017).

In this work, in order to improve the performance of Hem, we brought “electronic wires” AuNPs acting as a core to adsorb Hem molecules by biomineralization to accelerate the electron transferring and improve electrocatalytic activity by the synergistic effect of AuNPs and Hem (Scheme 1). Subsequently, a highly sensitive non-enzymatic electrochemical biosensor for the real-time detection of H_2O_2 was prepared based on the Hem@AuNPs/rGO/CS nanohybrids modified glassy carbon electrode (Hem@Au/rGO/CS/GCE). The integration of the catalysts highly enhanced the electrochemical properties via a comprehensive effect. To the best of our knowledge, this novel electrochemical biosensor was proposed for the first time to detect H_2O_2 in real-time with outstanding electrocatalytic features. Most importantly, the excellent properties such as low detection limit, wide linear range, high sensitivity and good stability, made it possible to detect H_2O_2 released from living cells with satisfactory result.

2. Experimental

2.1. Reagents and apparatus

Graphite powers (Macklin Biochemical Co., Ltd, Shanghai, China), $HAuCl_4{\cdot}3H_2O$ (Macklin Biochemical Co., Ltd, Shanghai, China), Hem (Yuanye biotechnology Co. Ltd, Shanghai, China), ascorbic acid (AA, Aladdin Chemistry Co., Ltd., Shanghai, China), NaOH (Fuchen chemical reagent Co., Ltd., Tianjin, China), and Hydrogen peroxide (H_2O_2, 30%, Fuchen chemical reagent Co., Ltd., Tianjin, China) were all used as received without any further purification. Phosphate buffer solution (PBS, 0.1 mol L^{-1}) were prepared using the mixture of the stock solutions (0.1 mol L^{-1} NaH_2PO_4 and Na_2HPO_4). A 2% (wt%) chitosan solution was prepared by dissolving 2.0 g chitosan into 100 mL 1.0% acetic acid and ultra-sonicated for 0.5 h at room temperature until complete dissolution.

Scanning electron microscope (SEM, Zeiss, sigma 500), Transmission electron microscope (TEM, FEI-Tecnai G2, USA) and UV-2550 spectrophotometer (Shimadzu, Japan) were applied to characterize the materials. A model CHI650B electrochemical workstation (Chenhua Instrument Company, Shanghai, China) was employed for electrochemical techniques with a traditional three-electrode system: a bare GCE or modified GCE (d = 4 mm) used as working electrode, a platinum (Pt) wire used as an auxiliary electrode and a saturated calomel electrode (SCE) used as a reference electrode, respectively.

2.2. Synthesis of GO and its reduction

Firstly, we prepared GO power by Hummers' method presented in previous report (Hummers and Offeman, 1958). Then, 50 mg mL^{-1} GO was dispersed in 10 mL deionized water and ultra-sonicated for 0.5 h. 500 mg reductant AA was added into GO solution and heated at 95 °C for 20 h. With the generation of flocculent rGO, the color of the mixture changed from claybank to black. The product was washed alternately with alcohol and deionized water by centrifuge at 7000 g. Finally, the obtained rGO was dried by freeze dryer and a 2 mg mL^{-1} stock solution of rGO was prepared for further use.

2.3. Synthesis of Hem@AuNPs/rGO nanocomposites

Hem@AuNPs were synthesized by gold biomineralization according to the previous work (Zhang et al., 2018) with slight modification. In brief, 10 mL 20 mM $HAuCl_4$ were mixed with 10 mL Hem solution (1.60 mg mL^{-1}). Then, 0.8 mg NaOH was added into the mixture until the concentration of NaOH reached 1.0 mol L^{-1}. Vigorous stirring was required in the whole operational process. After holding on 8 h at 37 °C, the Hem@AuNPs were purified by 20 KD ultrafiltration membrane and

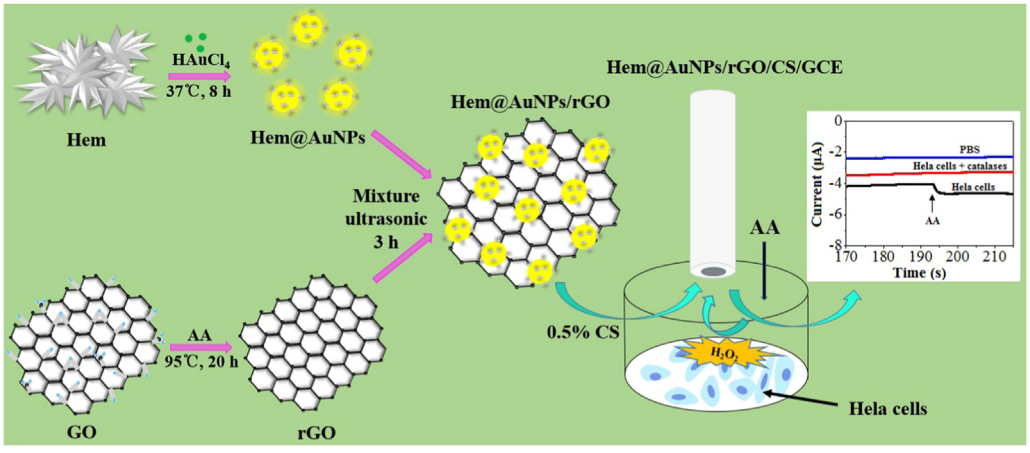

Scheme 1. Schematic illustration of the Hem@AuNPs/rGO/CS/GCE used for real-time detecting H_2O_2 released from Hela cells.

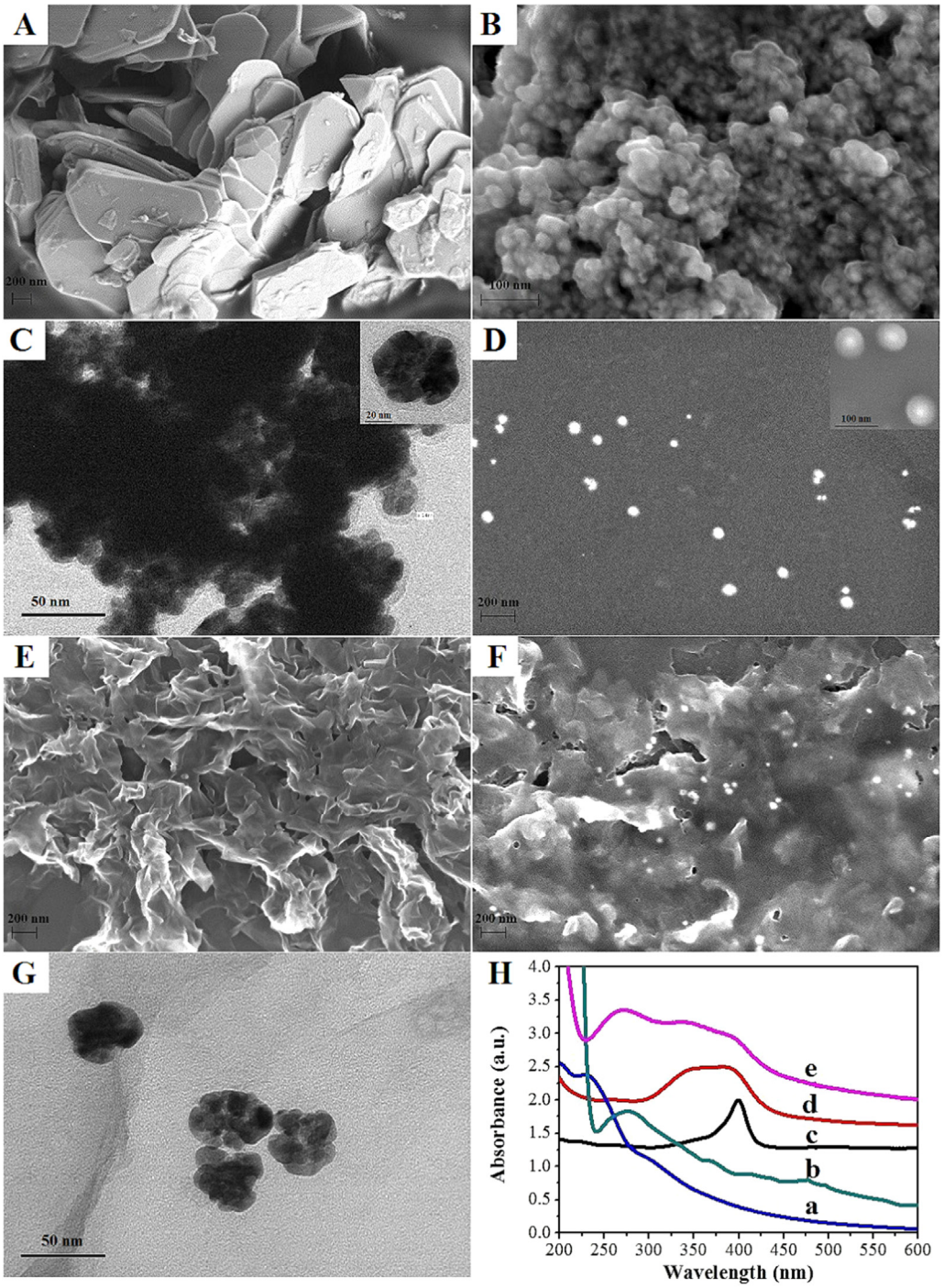

Fig. 1. SEM images of (A) Hem, (B) Hem@AuNPs freeze-dried powder, (D) Hem@AuNPs solution (insert: particles with magnitude-amplified view), (E) rGO, (F) Hem@AuNPs/rGO and TEM images of (C) Hem@AuNPs nanohybrids (insert: particles with magnitude-amplified view), (G) Hem@AuNPs/rGO. (H) UV–vis absorption spectra of GO (a), rGO (b), Hem (c), Hem@AuNPs (d) and Hem@AuNPs/rGO (e).

dried by freeze dryer. Similarly, the stock solution of Hem@AuNPs was also prepared as 2 mg mL^{-1}. Finally, Hem@AuNPs/rGO solution was prepared with the different volume ratios of Hem@AuNPs and rGO solution. The Hem@AuNPs/rGO solutions were ultra-sonicated for 3 h to make Hem@AuNPs uniformly attach on the surface of the rGO. The obtained 2 mg mL^{-1} Hem@AuNPs/rGO solutions were stored at 4 °C for further use.

2.4. Fabrication of H_2O_2 sensor

In order to immobilize nanohybrids on the GCE tightly, 6 mL Hem@AuNPs/rGO solution was mixed with 2 mL 2% CS solution due to the excellent film-forming property of CS. Thus, the proposed nanocomposites Hem@AuNPs/rGO/CS were ready with the final concentration of 1.5 mg mL^{-1} Hem@AuNPs/rGO and 0.5% chitosan. Prior to modification, the GCE was polished with 0.05 μm alumina powder until a mirror like surface was achieved, followed by ultrasound in alcohol and water successively. Next, 10 μL of Hem@AuNPs/rGO/CS suspension was deposited on the surface of GCE. After air-drying at room temperature, the desired biosensor was obtained and noted as Hem@AuNPs/rGO/CS/GCE. For comparison, Hem@AuNPs/CS/GCE, rGO/CS/GCE, Hem/CS/GCE and CS/GCE were fabricated with the

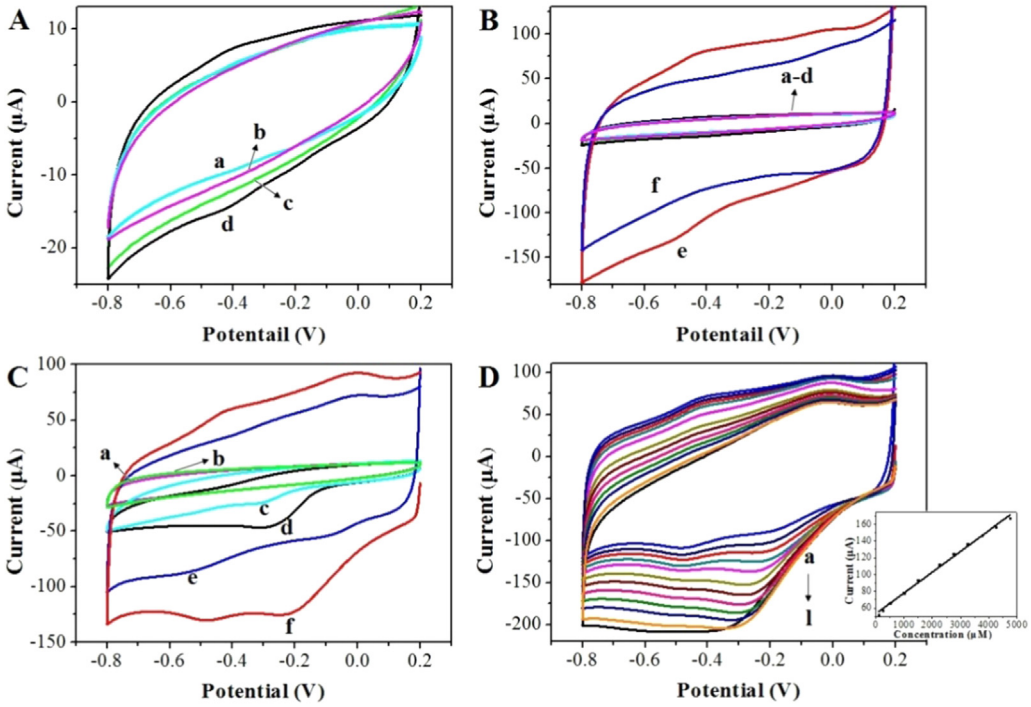

Fig. 2. (A) CVs of Hem/CS/GCE (a), bare/GCE (b), CS/GCE (c), Hem@AuNPs/CS/GCE (d) in N_2-saturated PBS. (B) CVs of Hem@AuNPs/rGO/CS/GCE (e) and rGO/CS/GCE (f) in N_2-saturated PBS. CVs of (a-d) were corresponding to the curves in (A). (C) CVs of bare GCE (a), CS/GCE (b), Hem/CS/GCE (c), Hem@AuNPs/CS/GCE (d), rGO/CS/GCE (e) and Hem@AuNPs/rGO/CS/GCE (f) in the presence of 500 μM H_2O_2 in N_2-saturated PBS. (D) CVs of H_2O_2 with different concentrations of (a-l) 100 μM, 250 μM, 500 μM, 1000 μM, 1500 μM, 2250 μM, 2750 μM, 3250 μM, 3750 μM, 4250 μM and 4750 μM at Hem@AuNPs/rGO/CS/GCE in N_2-saturated PBS. Inset shows the linear relation of peak current with the concentrations of H_2O_2. Scan rate: 50 mV s^{-1}, pH = 7.0.

similar procedure.

2.5. Cell culture

The cells used in this experiment were Hela cells (human cervical cancer cells). They were cultured in Dulbecco's Modified Eagle Medium containing 10% heat-inactivated fetal calf serum (Sigma-Aldrich, St. Louis, MO, USA), 100 U/mL penicillin (Sigma-Aldrich) and 100 mg mL^{-1} streptomycin (Sigma-Aldrich). The culture was performed at 37 °C in a 95% humid atmosphere with 5% carbon dioxide.

2.6. Electrochemical detection of H_2O_2 released from cells

Hela cells were seeded and grown in the cell culture plate with the diameter of 35 mm (1.0×10^6 cells). Cell number was estimated by a cell counter. The culture medium was removed and the cells were washed by the deoxygenated PBS buffer (0.01 M, pH 7.4) for three times. Then 1 mL N_2-saturated PBS (0.1 M, pH 7.4) was added for the electrochemical measurements. The Hem@AuNPs/rGO/CS/GCE was immersed in the cell solution and used for the amperometric detection of H_2O_2 in Hela cells. When 1×10^{-6} mol L^{-1} AA was injected into the suspension, it can motivate the cells releasing H_2O_2 into the PBS (Zhang et al., 2013a). The proposed biosensor can respond the H_2O_2 in real-time and transform this response into electrochemical signal.

3. Results and discussion

3.1. Synthesis and characterization of Hem@AuNPs/rGO/CS composites

It has been reported that Hem possesses the peroxidase-like catalysis, but some shortages limited its utilization. In the present work, we improved the electrocatalytic activity of Hem by anchoring it onto biomineralized AuNPs to form Hem@AuNPs nanohybrids, followed by being dispersed and attached onto the surface of rGO. In order to immobilize on the GCE more tightly, CS was introduced to the Hem@AuNPs/rGO. The synthesis and utilization of the nanohybrids are shown in Scheme 1. Herein, the biomineralized AuNPs acted as "nanowires" to promote the electron shuttling of the catalysis-active site of Hem. The electrochemical property was improved at the first stage benefiting from the synergistic effect of AuNPs and Hem. At the second stage, the electrocatalytic activity was further promoted when rGO was brought into the composites. On one hand, the large surface area can adsorb more Hem@AuNPs. On the other hand, the strong conductivity of rGO can enhance electron transfer once again. Finally, the induction of CS can form protective films to increase the stability of the proposed biosensor.

The morphological characterization of the nanohybrids was performed by SEM. In general, the original Hem is flake-like with variety of shapes (Fig. 1A). After reaction together with $HAuCl_4$, its morphology changed completely. The morphology of the Hem@AuNPs freeze-dried powder (Fig. 1B and C) exhibited a thin semitransparent film covering on the surface of solid nanoparticles, indicating that crowds of Hem molecules were wrapped around the surface of bigger AuNPs which were formed in site by Hem-mediated biomineralization. The Hem@AuNPs nanohybrids were easy dispersed in water with uniform sizes and original morphosis (Fig. 1D). The inset in Fig. 1C and D is a larger version of Hem@Au which explains the structure more clearly. In addition, rGO presented membrane-like structure with a lot of random wrinkles and rolled edges (Fig. 1E) which could increase its surface area. After ultrasonication together, the Hem@Au nanoparticles were stabilized on the surface of rGO nanosheets uniformly (Fig. 1F and G). Moreover, the micrographs of Hem@AuNPs/rGO/CS exhibited that the membranous CS covered on Hem@AuNPs/rGO with rough surface (Fig. S1A and S1B).

The UV–vis spectra of the composites are shown in Fig. 1H. In the spectra of GO (curve a), the absorption at approximately 233 nm was corresponding to π–π* transitions of the aromatic C=C band. Moreover, shoulder absorption at about 300 nm was attributed to n–π* transitions of the C=O band. After reduction (curve b), the absorption at 233 nm was red-shifted to 267 nm and the absorption at 300 nm disappeared, demonstrating the restoration of sp^2 structure and the formation of rGO. The spectra of the Hem solution exhibited a strong absorption band at 400 nm corresponding to the Soret band of Hem (curve c). When Hem was remolded with the biomineralized gold and formed the Hem@AuNPs (curve d), both of the absorbance peaks of Hem and biomineralized gold (335 nm) could be observed, which confirmed the

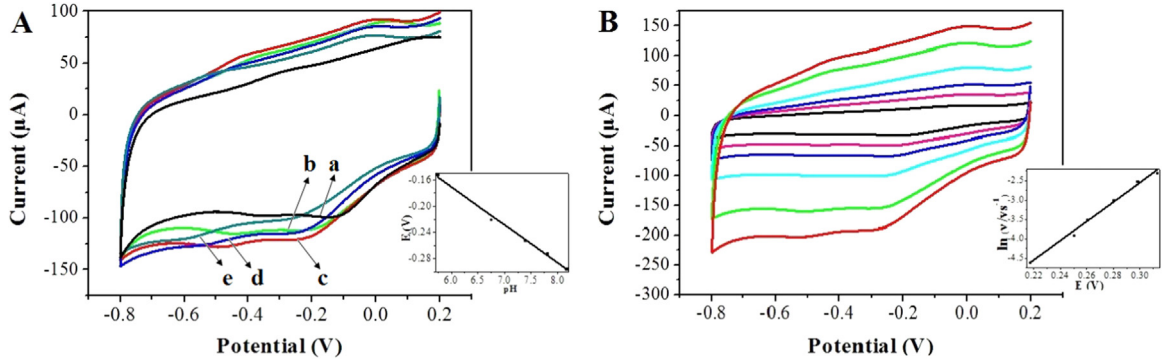

Fig. 3. (A) Superimposed CVs of 500 μM H_2O_2 in N_2-saturated PBS with different pH of (a–e) 5.74, 6.74, 7.40, 7.80 and 8.16. Scan rate: 50 mVs^{-1}. Inset: Relation between peak potentials and solution pH. (B) Superimposed CVs of 500 μM H_2O_2 in N_2-saturated PBS (pH 7.4) with different scan rates of (from a to f) 10, 20, 30, 50, 80 and 100 mV s^{-1}. Inset: Linear relationship of E_P and ln ν.

formation of Hem@AuNPs. Moreover, the Hem@AuNPs/rGO displayed all the characteristic absorptions of Hem, biomineralized gold and rGO (curve e), indicating that the Hem@AuNPs/rGO nanohybrids was synthesized successfully.

3.2. Electrochemical behaviors of the Hem@AuNPs/rGO/CS nanohybrids modified electrode

Electrochemical properties of the nanohybrids were researched by cyclic voltammograms (CVs). In the absence of H_2O_2, the CV curves of CS, Hem/CS, Hem@AuNPs/CS was overlaid in Fig. 2A and CV curves of rGO/CS, Hem@AuNPs/rGO/CS was overlaid in Fig. 2B. As shown in Fig. 2A, no redox peak appeared on the bare GCE (curve b) and CS/GCE (curve c). When Hem/CS covered on the surface of GCE, there was still no obvious redox peaks (curve a), which might because of the poor conductivity or less amount of Hem. After Hem attached on the biomineralized AuNPs, a pair of redox peaks appeared obviously (curve d). These peaks at about −0.43 V should be ascribed to the redox of iron at the core of Hem, revealing that the introduction of AuNPs could greatly facilitate the electron transfer between Hem and the electrode. For further enhancing the performance of the biosensor, we brought rGO to adsorb Hem@AuNPs. The redox peaks of Hem were increased greatly on Hem@AuNPs/CS/GCE (Fig. 2B, curve e), indicating that the electron transfer can be improved once again. By contrast, rGO/CS/GCE gave no desired peaks except a pair of weak peaks at about −0.05 V (Fig. 2B, curve f) which related to the redox reactions of some oxygenated functional groups (in this case, OH) on rGO.

Furthermore, these modified electrodes were used to investigate the electrocatalytic activity toward the reduction of H_2O_2 (Fig. 2C). When 500 μM H_2O_2 was injected into the N_2-saturated PBS (0.1 M, pH 7.4), there was still no obvious peaks observed on bare GCE (curve a) and CS/GCE (curve b). Besides, a weak reduction peak appeared at about −0.6 V on rGO/GCE (curve e). However, when Hem/CS coated on the GCE, there was an obvious peak appeared at −0.34 V (curve c). This peak was attributed to the reduction of H_2O_2 by the catalysis of Hem. In addition, the peak increased sharply on Hem@AuNPs/CS/GCE (curve d), indicating that the electrocatalytic activity was improved by the synergistic effect of Hem and AuNPs. Moreover, the current of the reduction peak reached the maximum at the Hem@AuNPs/rGO/CS modified GCE (curve f), attributing to the excellent electrocatalytic activity of Hem@AuNPs and high conductivity of rGO. In addition, we further researched the electrocatalytic behavior of Hem@AuNPs/rGO/CS/GCE towards the increasing H_2O_2 (Fig. 2D). The current of the reductive peak continued to increase linearly with the gradually addition of H_2O_2 (inset in Fig. 2D) until the concentration of H_2O_2 reached 4250 μM. This phenomenon further demonstrated that Hem@AuNPs/rGO nanohybrids exhibited an outstanding electrocatalytic activity towards the reduction of H_2O_2 with a high sensitivity and could be used in the electrochemical detection of H_2O_2. Moreover, as the concentration of H_2O_2 increased, the reduction peak shifted to negative potential slightly, which might result from the torpid electron transfer kinetics (Wang et al., 2015; Zhou et al., 2017).

3.3. Influence of the ratio of Hem@AuNPs:rGO, solution pH and scan rates

In order to obtain the best catalytic effect, we explored the optimum ratio of Hem@AuNPs:rGO. The different Hem@AuNPs/rGO solutions with various volume ratios of Hem@AuNPs and rGO were mixed with CS solution and then used for the CV analysis towards H_2O_2. When the volume ratios of Hem@AuNPs and rGO increased from 1:59 to 30:30, the reduction currents of H_2O_2 enhanced at first and then decreased (Fig. S2). The peak current reached the maximum when the proportion of Hem@AuNPs and rGO was 5:55, indicating that the comprehensive effect towards H_2O_2 reduction reached optimum when 5 portions of Hem@AuNPs attached on 55 portions of rGO. The ratio 5:55 was chose as the best ratio and used in the further research without special version.

To explore the reaction mechanism on the proposed electrode, we researched the electrochemical behaviors of H_2O_2 with different pH and various scan rates (ν). With the pH of supporting electrolyte increasing from 5.74 to 8.16, the response potentials of H_2O_2 shifted slightly towards the negative potential (Fig. 3A), indicating that protons were directly involved in the electrode reaction. Moreover, as shown in inset of Fig. 3A, there was a good linear relationship between peak potential and pH with the linear equation of E_P (V) = 0.0578 pH − 0.176, R^2 = 0.9941. Obviously, the slope 0.0578 V pH^{-1} was close to the theoretical value 0.059 V pH^{-1}, explaining that equal numbers of electron and proton took part in the peak redox. Simultaneously, the peak current at pH 7.4 was a little higher than that at other pH (Fig. S3), indicating the catalytic activity of this biosensor is more effective at pH 7.4, which is consistent with the real conditions of biological systems. Thus pH 7.4 PBS was selected for H_2O_2 detection.

The influence of scan rates on the reduction peak of H_2O_2 was examined at the range from 0.01 V s^{-1} to 0.1 V s^{-1}. With the increasing of scan rates, the peak potential moved to negative direction gently and the peak current increased simultaneously (Fig. 3B). In addition, the peak potential and the logarithm of scan rate showed a linear relationship (inset in Fig. 3B) with the equation: E_P (V) = 25.01 ln (ν/V s^{-1}) - 10.05, R^2 = 0.9923. According to Laviron's model (Eq. (1)) (Laviron, 1979), the number of the electron (n) involved in the reaction was calculated to be 2 by assuming an electron transfer coefficient α = 0.5. That is, there were two protons and two electrons involved in the electrode reaction.

$$E_P(V) = E^{0'} - \frac{RT}{\alpha nF} \ln \frac{RTk_s}{\alpha nF} + \frac{RT}{\alpha nF} \ln \nu \quad (1)$$

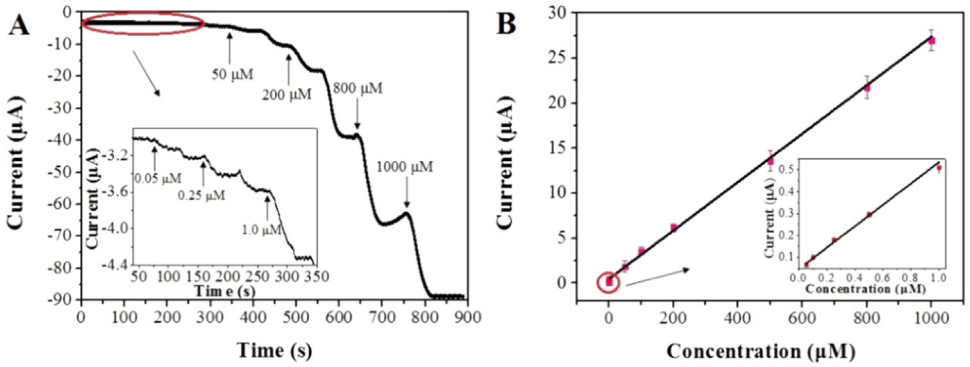

Fig. 4. (A) Typical *i*–t curves with successive additions of H_2O_2 at an applied potential of −0.3 V. Inset: Amplified response from 50 s to 350 s (B) Linear calibration of *i*–t. Inset: linear calibration at low concentration from 0.05 μM to 1 μM.

where $E^{0'}$ is the formal standard potential, and ν, R, F and T represent their usual meaning.

Based on the above results and previous researches (Devi and ArunaKumari, 2013; Zhang et al., 2013b), a simplified reaction mechanism of Hem@AuNPs/rGO/CS/GCE electrocatalysis towards H_2O_2 was presumed reasonably:

$$\text{Au-Hem } (Fe^{3+}) + H_2O_2 \rightarrow \text{Compound I } (Fe^{4+} = O) + H_2O$$

$$\text{Compound I } (Fe^{4+} = O) + H^+ + e^- \rightarrow \text{Compound II}$$

$$\text{Compound II} + H^+ + e^- \rightarrow \text{Au-Hem } (Fe^{3+}) + H_2O$$

3.4. Amperometric response of Hem@AuNPs/rGO/CS towards H_2O_2

Under the optimal experimental conditions, the biosensor for electrochemical determination of H_2O_2 was developed based on amperometric method. Fig. 4A displays the *i*–t curve recorded by Hem@AuNPs/rGO/CS/GCE biosensor at the applied potential of −0.3 V. The enlarged view of the *i*–t response towards the H_2O_2 with the lower concentrations was shown in the inset of Fig. 4A. Each time with the H_2O_2 addition, the current changed steeply from a stable-state to reach a new stable-state within 50 s, suggesting the rapidly response of the proposed biosensor towards H_2O_2. The current signal of the biosensor increased along with H_2O_2 concentrations and demonstrated two linear ranges (Fig. 4B). At the higher concentrations from 1.0 μM to 1000 μM, the linear regression equation was i_P (μA) = 0.0269c (μM) + 0.4877 with a correlation coefficient of 0.9992. At the lower concentrations from 0.05 μM to 1.0 μM (inset in Fig. 4B), the linear regression equation was i_P (μA) = 0.4885c (μM) + 0.0462 with a correlation coefficient of 0.9972. The limit of detection (LOD) was calculated to be 0.0094 μM (S/N = 3). Compared with the other Hem-based electrochemical sensors and some spectrometry methods towards H_2O_2 detection, the proposed biosensor exhibited some obvious advantages such as lower detection limit and wider linear ranges (Tables S1 and S2).

3.5. Selectivity, reproducibility and stability of the biosensor

In order to assess the practicability of the proposed H_2O_2 biosensor, it is necessary to investigate the selectivity in the presence of some potential interferences. Herein, the possibly coexisting interferences, such as AA, dopamine (DA), uric acid (UA), cysteine (Cys) and glucose (Glu) were introduced under the same conditions. As shown in Fig. S4, the signal increase were mainly caused by the twice addition of 500 μM H_2O_2 at about 120 s and 330 s, respectively. When 10 folds of AA, DA, UA, Cys and Glu were injected into the same substrate solution, there was hardly any response at the Hem@AuNPs/rGO/CS/GCE, illustrating that this developed biosensor was highly selective for H_2O_2.

The reproducibility and stability were also researched. For the five determinations using the same biosensor, the response current is almost unchanged with a relative standard deviation (RSD) of 1.47%, suggesting good repeatability of the proposed method. Moreover, the RSD of five independent sensors was 1.8%, explaining excellent reproducibility of the modified electrode. After the electrode was stored at 4 °C for seven days, the peak current of H_2O_2 decreased to 95.4%, illustrating the good stability of the proposed biosensor.

3.6. Detection of H_2O_2 released from living cells

Generally, H_2O_2 in the normal cells possesses a low concentration. Once normal cells transform into tumor cells, they will produce more H_2O_2 rapidly. So H_2O_2 is a potential marker for tumor cells (Sun et al., 2012). Disturb by a proper amount of AA can motivate the living cells releasing H_2O_2 into the extracellular matrix. In this work, Hela cells were chose as the model cancer cell, and Hem@AuNPs/rGO/CS/GCE was used to real-time detection of H_2O_2 released from the living cells owing to its highly electrocatalytic activity. Fig. 5 records the *i*–t curves obtained by Hem@AuNPs/rGO/CS/GCE at an applied potential of −0.3 V under different conditions. When 1 μM AA was injected into the blank PBS (curve a), there was no obvious wave at the *i*–t curve, explaining that AA was no disturb to the biosensor. In the PBS with the presence of Hela cells (curve c), the addition of AA could cause a significant response, which demonstrated that H_2O_2 can be released from Hela cells and reduced on Hem@AuNPs/rGO in real-time. In order to confirm whether the increased current signal was caused by the H_2O_2, the catalase, a selective scavenger of H_2O_2, was added to the PBS containing Hela cells. As expected, the response disappeared due to the decomposition of H_2O_2 (curve b), revealing that the current change was indeed ascribed to the electrochemical reduction of H_2O_2 released from the living cells. The peak current was about 0.63 μA (n = 3, curve c), corresponding to 5.04 μM H_2O_2, which was highly consistent with the

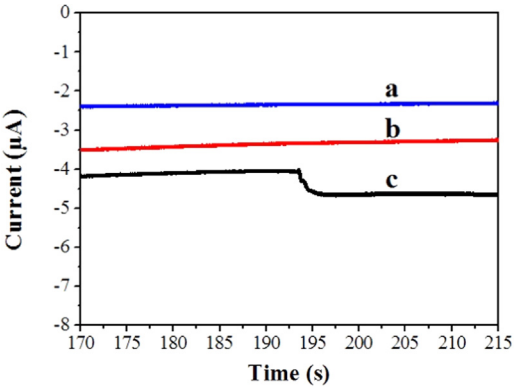

Fig. 5. Amperometric response of H_2O_2 released from Hela cells stimulated by AA at −0.3 V. (a) PBS; (b) 1×10^6 Hela cells and 300 U/mL catalases in PBS; (c) 1×10^6 Hela cells in PBS.

previous report (Ma et al., 2018). Thus, we can affirm that Hem@AuNPs/rGO/CS/GCE had an ultrasensitive electrochemical response and could be effectively used for the real-time detection of H_2O_2 in living cells. In addition to living cells, the proposed H_2O_2 sensor can also be used in other real samples, such as in the serum and disinfectant (Fig. S5).

4. Conclusion

In summary, we have fabricated a non-enzymatic H_2O_2 biosensors based on the highly electrocatalysis activity of Hem@AuNPs, excellent conductivity of rGO and good film-forming property of CS. These advantages made the proposed biosensor possible to determine H_2O_2 in real-time with outstanding sensitivity, good selectivity and long-term stability. In addition, the proposed biosensor exhibited detection limit of 9.3 nM and wider linear range from 0.05 μM to 1.0 μM and 1.0 μM to 1000 μM. Moreover, the biosensor can further detect the H_2O_2 released from living Hela cells with a satisfactory result. Although the preparation of this biosensor was a little complicated, this work still provided a great possibility for the application of Hem@AuNPs/rGO/CS/GCE to monitor the generation of H_2O_2 in living cells.

CRediT authorship contribution statement

Wenjing Wang: Conceptualization, Methodology, Formal analysis, Validation, Investigation, Data curation, Writing - original draft. **Huabiao Tang:** Investigation, Visualization, Writing - review & editing. **Yuan Wu:** Visualization. **Yinli Zhang:** Resources. **Zhaohui Li:** Conceptualization, Supervision, Project administration, Funding acquisition, Writing - review & editing.

Acknowledgments

This work was supported in part by the National Natural Science Foundation of China (21205108), the Foundation for University Key Teacher by Henan Province (2017GGJS007), the Key Scientific Research Project in Universities of Henan Province (19A150048), and the Fundamental Research Funds for the Central Universities from Hunan University.

Credit authorship Taxonomy statement

Wenjing Wang: Conceptualization, Methodology, Formal Analysis, Validation, Investigation, Data Curation, Writing-Original Draft. **Huabiao Tang**: Investigation, Visualization, Writing-Reviewing and Editing. **Yuan Wu**: Visualization. **Yinli Zhang**: Resources. **Zhaohui Li**: Conceptualization, Supervision, Project Administration, Funding Acquisition, Writing-Reviewing and Editing.

Declaration of interests

none

Appendix A. Supporting information

Supplementary data associated with this article can be found in the online version at doi:10.1016/j.bios.2019.02.039.

References

Afkhami, A., Hashemi, P., Bagheri, H., Salimian, J., Ahmadi, A., Madrakian, T., 2017. Biosens. Bioelectron. 93, 124–131.
Bai, Z.H., Li, G.Y., Liang, J.T., Su, J., Zhang, Y., Chen, H.Z., Huang, Y., Sui, W.G., Zhao, Y.X., 2016. Biosens. Bioelectron. 82, 185–194.
Berbec, S., Zoladek, S., Jablonska, A., Palys, B., 2018. Sens. Actuator B Chem. 258, 745–756.
Bhunia, S.K., Dolai, S., Sun, H.C., Jelinek, R., 2018. Sens. Actuator B Chem. 270, 223–230.
Cao, Y., Si, W.M., Hao, Q.L., Li, Z.F., Lei, W., Xia, X.F., Li, J., Wang, F.G., Liu, Y.Y., 2018. Electrochim. Acta 261, 206–213.
Chang, H.H., Lv, J., Zhang, H.C., Zhang, B., Wei, W.L., Qiao, Y., 2017. Biosens. Bioelectron. 87, 579–586.
Chen, D.D., Zhuang, X.M., Zhai, J., Zheng, Y.Y., Lu, H., Chen, L.X., 2018. Sens. Actuator B Chem. 255, 1500–1506.
Devi, L.G., ArunaKumari, M.L., 2013. Appl. Surf. Sci. 276, 521–528.
Drmosh, Q.A., Yamani, Z.H., Hendi, A.H., Gondal, M.A., Moqbel, R.A., Saleh, T.A., Khan, M.Y., 2019. Appl. Surf. Sci. 464, 616–626.
Fleury, C., Mignotte, B., Vayssiere, J.L., 2002. Biochimie 84 (2–3), 131–141.
Gupta, R., Singh, P., Ganesan, V., Koch, B., Rastogi, P.K., Yadav, D.K., Sonkar, P.K., 2018. Sens. Actuator B Chem. 276, 517–525.
Halliwell, B., Chirico, S., 1993. Am. J. Clin. Nutr. 57 (5 Suppl), 715S–724S (discussion 724S-725S).
He, B.B., Ma, Y.P., Gong, X.X., Long, Z.N., Li, J.S., Xiong, Q., Liu, H., Chen, Q., Zhang, X.H., Yang, S.Z., Liu, Q.H., 2017. J. Phys. D Appl. Phys. 50 (44), 9.
Hu, A.L., Liu, Y.H., Deng, H.H., Hong, G.L., Liu, A.L., Lin, X.H., Xia, X.H., Chen, W., 2014. Biosens. Bioelectron. 61, 374–378.
Hummers, W.S., Offeman, R.E., 1958. Prep. Graph. Oxide.
Jha, S.K., Kumar, C.N., Raj, R.P., Jha, N.S., Mohan, S., 2014. Electrochim. Acta 120, 308–313.
Laviron, E., 1979. J. Electroanal. Chem. 101 (1), 19–28.
Lebiga, E., Fernandez, R.E., Beskok, A., 2015. Analyst 140 (15), 5006–5011.
Li, M.D., Wang, P., Li, F.Y., Chu, Q.Y., Li, Y.Y., Dong, Y.H., 2017. Biosens. Bioelectron. 87, 752–759.
Lim, S.D., Sun, C., Lambeth, J.D., Marshall, F., Amin, M., Chung, L., Petros, J.A., Arnold, R.S., 2005. Prostate 62 (2), 200–207.
Luo, X.L., Xu, J.J., Zhang, Q., Yang, G.J., Chen, H.Y., 2005. Biosens. Bioelectron. 21 (1), 190–196.
Ma, B., Kong, C.C., Hu, X.X., Liu, K., Huang, Q., Lv, J., Lu, W.J., Zhang, X.J., Yang, Z.M., Yang, S., 2018. Biosens. Bioelectron. 106, 29–36.
Pakchin, P.S., Ghanbari, H., Saber, R., Omidi, Y., 2018. Biosens. Bioelectron. 122, 68–74.
Policastro, L., Molinari, B., Larcher, F., Blanco, P., Podhajcer, O.L., Costa, C.S., Rojas, P., Dur n, H., 2004. Mol. Carcinog. 39 (2), 103–113.
Rizwan, M., Elma, S., Lim, S.A., Ahmed, M.U., 2018. Biosens. Bioelectron. 107, 211–217.
Santos, S.R., Maia, G., 2012. Electrochim. Acta 71, 116–122.
Song, M.R., Wang, J.L., Chen, B.Y., Wang, L., 2017. Anal. Chem. 89 (21), 11537–11544.
Sun, X.L., Guo, S.J., Liu, Y., Sun, S.H., 2012. Nano Lett. 12 (9), 4859–4863.
Valavanidis, A., Vlachogianni, T., Fiotakis, C., 2009. J. Environ. Sci. Health Pt. C Environ. Carcinog. Ecotoxicol. Rev. 27 (2), 120–139.
Valko, M., Izakovic, M., Mazur, M., Rhodes, C.J., Telser, J., 2004. Mol. Cell. Biochem. 266 (1–2), 37–56.
Wang, B.B., Ji, X.P., Ren, J.J., Ni, R.X., Wang, L., 2017. Bioelectrochemistry 118, 75–82.
Wang, L., Zhang, Y.Y., Cheng, C.S., Liu, X.L., Jiang, H., Wang, X.M., 2015. ACS Appl. Mater. Interfaces 7 (33), 18441–18449.
Wang, T.Y., Zhu, H.C., Zhuo, J.Q., Zhu, Z.W., Papakonstantinou, P., Lubarsky, G., Lin, J., Li, M.X., 2013. Anal. Chem. 85 (21), 10289–10295.
Wei, Y.H., 1998. Proceedings of the society for experimental biology and medicine. Soc. Exp. Biol. Med. 217 (1), 53–63 (New York, N.Y.).
Ye, Y.K., Gao, J.N., Zhuang, H., Zheng, H.S., Sun, H.J., Ye, Y.W., Xu, X., Cao, X.D., 2017. Microchim. Acta 184 (1), 245–252.
Zhai, X.R., Li, Y.H., Li, J.S., Yue, C.Y., Lei, X.W., 2017. Mater. Sci. Eng. C Mater. Biol. Appl. 77, 1242–1246.
Zhang, F.T., Long, X., Zhang, D.W., Sun, Y.L., Zhou, Y.L., Ma, Y.R., Qi, L.M., Zhang, X.X., 2014. Sens. Actuator B Chem. 192, 150–156.
Zhang, L.Y., Fan, C., Liu, M., Liu, F.J., Bian, S.S., Du, S.Y., Zhu, S.Y., Wang, H., 2018. Sens. Actuator B Chem. 266, 543–552.
Zhang, Y., Wu, C.Y., Zhou, X.J., Wu, X.C., Yang, Y.Q., Wu, H.X., Guo, S.W., Zhang, J.Y., 2013a. Nanoscale 5 (5), 1816–1819.
Zhang, Y., Xia, Z., Liu, H., Yang, M.J., Lin, L.L., Li, Q.Z., 2013b. Sens. Actuator B Chem. 188, 496–501.
Zhou, J., Zhao, Y.N., Bao, J., Huo, D.Q., Fa, H.B., Shen, X., Hou, C.J., 2017. Electrochim. Acta 250, 152–158.